Single-cell quantification of molecules and rates using open-source microscope-based cytometry

Andrew Gordon[1,2], Alejandro Colman-Lerner[1,2], Tina E Chin[1], Kirsten R Benjamin[1], Richard C Yu[1] & Roger Brent[1]

Microscope-based cytometry provides a powerful means to study cells in high throughput. Here we present a set of refined methods for making sensitive measurements of large numbers of individual *Saccharomyces cerevisiae* cells over time. The set consists of relatively simple 'wet' methods, microscope procedures, open-source software tools and statistical routines. This combination is very sensitive, allowing detection and measurement of fewer than 350 fluorescent protein molecules per living yeast cell. These methods enabled new protocols, including 'snapshot' protocols to calculate rates of maturation and degradation of molecular species, including a GFP derivative and a native mRNA, in unperturbed, exponentially growing yeast cells. Owing to their sensitivity, accuracy and ability to track changes in individual cells over time, these microscope methods may complement flow-cytometric measurements for studies of the quantitative physiology of cellular systems.

Single-cell measurements can reveal information obscured in population averages. For example, studies of variation in gene expression in individual *Escherichia coli* and *S. cerevisiae*[1,2] cells have shown that only a fraction of cell-to-cell variation in the expression of reporter genes results from stochastic fluctuations in the workings of the gene expression machinery[3–5], and have identified other processes and genes that account for and control the bulk of the variation[3].

One means to collect single-cell data is flow cytometry, whose development began in the 1930s (ref. 6). Modern instruments are powerful[6] but (i) cannot interrogate individual cells repeatedly to produce time series for each cell, (ii) cannot collect a great deal of light, owing to both the short time (typically microseconds) that the cell passes the detector, and to the numerical aperture of the objective, which often collects less than 10% of the emitted light, and (iii) typically do not capture images of the cells, making it difficult to analyze cell shape, size and intracellular localization of fluorescence. Some recent work has attempted to address the last two limitations by integrating the fluorescence signal over longer times and capturing cell images with custom-built charge-coupled device (CCD) detectors[7].

Optical microscopy can compensate for some limitations of flow cytometry by providing abilities to revisit individual cells over time, collect emitted light for long times and capture cell images with high resolution. Automation by computer-aided cell tracking and image analysis, as begun in the 1960s, permits generation of such data with high throughput[8–13]. During the past 20 years, a good deal of research-directed automated microscope-based cytometry outside of clinical and pharmaceutical applications has relied on two commercial software packages, Metamorph (Molecular Devices Corporation) and ImagePro (Media Cybernetics, Inc.), to operate the microscopes, collect the data and analyze them. These packages, often used together with more general purpose analysis programs, such as Matlab (The Mathworks, Inc.) and Labview (National Instruments Corporation), probably constitute the state of the art in commercial software used for these purposes. Likewise, open-source projects can provide valuable tools for image analysis. Examples include the Open Microscopy Environment (OME), which provides file formats and metadata standards for microscope images[14], Image J, a Java-based package of microscope image analysis tools[15], and CellProfiler[16].

Here we describe a suite of user-modifiable, technical and analytical methods to facilitate accurate, high-throughput measurements from single cells over time. The methods each derive from relatively well-known techniques but combine to produce a powerful, open-source microscope-based cytometry. The methods work with single yeast cells and mammalian lymphocytes, and can be altered for other cell types. When used with inexpensive optical microscopes and high-quality CCD equipment, these methods allowed fluorescence measurements more sensitive than those from contemporary flow cytometers, and allowed scoring, quantification and extraction of meaningful statistics from 1–2 fluorescent protein molecules per pixel in single-cell images. We used these methods to calculate maturation rates of fluorescent protein derivatives in single cells and develop single-image, 'snapshot' experiments to calculate degradation rates of fluorescent protein derivatives in exponentially growing cultures.

[1]The Molecular Sciences Institute, 2168 Shattuck Avenue, Berkeley, California 94704, USA. [2]These authors contributed equally to this work. Correspondence should be addressed to A.G. (agordon@molsci.org), A.C.-L. (colman-lerner@molsci.org) or R.B. (brent@molsci.org).

RECEIVED 6 SEPTEMBER 2006; ACCEPTED 20 DECEMBER 2006; PUBLISHED ONLINE 21 JANUARY 2007; DOI:10.1038/NMETH1008

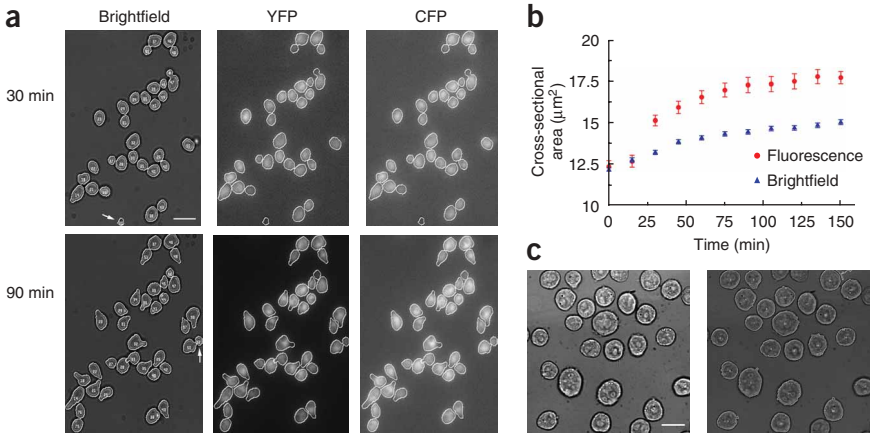

Figure 1 | Quantitative information extracted by Cell-ID. (**a**) Sample brightfield and corresponding YFP and CFP fluorescence images of TCY3154 yeast (containing P_{ACT1}-*CFP* and P_{PRM1}-*YFP* reporters) at 30 and 90 min after treatment with 20 nM α factor. White lines are cell boundaries found by Cell-ID. Assigned identifier numbers in the brightfield images (not readable in the images shown) are output by Cell-ID. A cell marked by a white arrow in the 30 min image is a false positive, spurious cell, and two cells in the bottom left of the 90-min image, which do not appear in the 30 min image, are unattached cells that settled into the visual field after the 30 min time point. The cell marked by a white arrow in the 90 min image is a newly identified cell, which appears as a slightly out-of-focus bud in the corresponding 30-min image. Fluorescence intensities are scaled to aid visualization. (**b**) Average cross-sectional area of populations of cells (error bars, 1 s.e.m.; $n = 60$ for fluorescence and $n = 470$ for brightfield) treated with 20 nM pheromone at $T = 0$ followed by cycloheximide at $T = 30$ min as determined with Cell-ID using the brightfield or the fluorescence image. (**c**) Sample brightfield image of human HL-60 cells before (left) and after (right) Cell-ID located and uniquely identified each cell. Scale bars, 10 μm.

RESULTS

Open-source, microscope-based, time-course cytometry

The method required capabilities to (i) image fields of living cells and return to each field reliably over time, (ii) determine automatically the correct focus for each field using a brightfield image, (iii) automatically identify and track cells in the images, (iv) extract quantitative information from the tracked cells, and (v) analyze large data sets that comprise numerous measurements associated with individual cells. These capabilities rest on relatively simple microscope methods and, in two cases, on relatively sophisticated software. We detail in the **Supplementary Note** online the microscope methods, the relatively simple autofocus software and our use of a powerful open-source data analysis program, Physics Analysis Workstation (PAW), developed over the past 20 years at the European Center for Nuclear Research (CERN). Here we briefly describe the other software, Cell-ID 1.0 (**Supplementary Software** online)—which we wrote to track and identify cells—and how we used it to measure total cell fluorescence, fluorophore maturation rates as well as protein and mRNA decay rates.

Cell-ID 1.0 uses brightfield images to identify cells, assigns a unique identifier number to each cell, scores interior and boundary pixels, tracks the cells through time-series of images and, in conjunction with fluorescence images, calculates various cellular

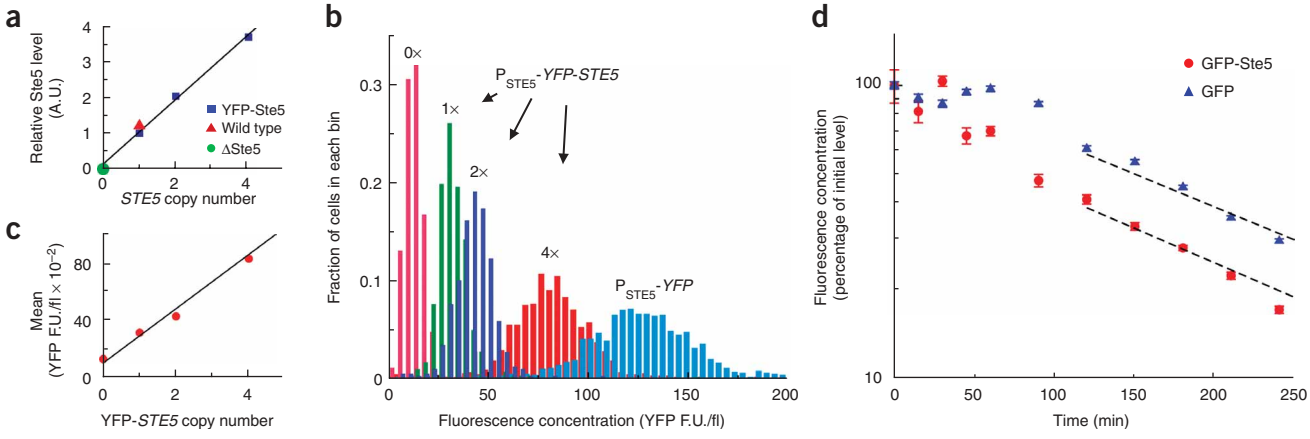

Figure 2 | Steady-state distributions of YFP and YFP-Ste5. (**a**) Level of Ste5 protein as determined by quantitative western blot as a function of the number of integrated copies of P_{STE5}-*YFP-STE5* and for wild-type cells and ΔSte5 cells, relative to the 1× strain. The line corresponds to a linear fit. (**b**) Single-cell distribution of fluorescence in cells that had been growing exponentially for more than 15 h, for strains that expressed native Ste5 from the endogenous promoter (0×), strains containing 1 copy of P_{STE5}-YFP-STE5 (1×), 2 copies (2×), 4 copies (4×) integrated into the genome, and strains containing the *STE5* promoter driving YFP alone (P_{STE5}-*YFP*). (**c**) Mean fluorescence of 0×, 1×, 2× and 4× strains as a function of the number of copies of P_{STE5}-*YFP-Ste5*, with a linear fit overlaid. (**d**) Galactose shutoff experiments. We grew strains expressing P_{GAL1}-*GFP* and P_{GAL1}-*GFP-STE5* on glucose medium to exponential phase, diluted cells and grew them in galactose medium for > 24 h to induce the *GAL1* promoter, then transferred back to glucose to shut off the promoter (0 min). For each measurement, we fixed aliquots of these cultures with paraformaldehyde before imaging (**Supplementary Note**). Plot shows log of mean fluorescence concentration (fluorescence per unit volume) as a function of time after transfer of cells to glucose medium (error bars, 1 s.e.m.; *n* values range from 300 at $t = 0$ min to 1,000 at $t = 250$ min). Overlaid dotted lines indicate the reduction in fluorescence concentration expected exclusively from dilution through cell proliferation, as determined from exponential fits to OD measurements for the two strains.

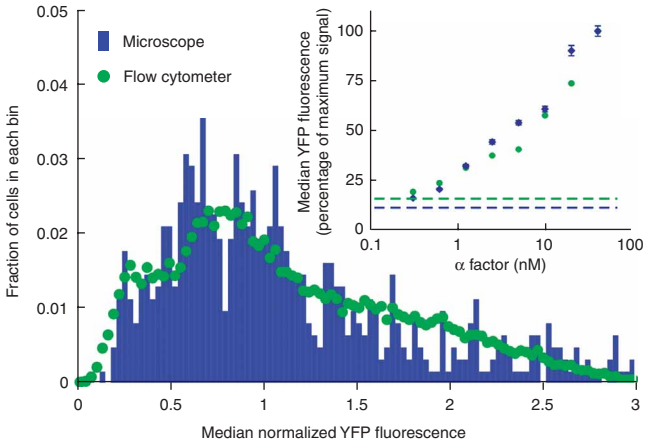

Figure 3 | Total fluorescence validation by comparison of Cell-ID–based measurements with flow cytometry. We treated cells containing the P_{PRM1}-*YFP* (strain ACLY387) construct with different concentrations of α factor for 90 min, fixed with 2% paraformaldehyde for 1 h, then washed twice in PBS and once in TE (10 mM Tris-HCl (pH 7.5), 1 mM EDTA)[3]. We used samples from these populations to measure YFP-derived fluorescence by microscopy using Cell-ID, and in parallel, by the LSR2 flow cytometer (excitation, 488 nm; emmission, 510–530 nm). Plot shows distribution of the total fluorescence in cells treated with 10 nM α factor. Data correspond to the median normalized fluorescence. Inset, α factor dose response obtained using Cell-ID and the flow cytometer. Data correspond to the median of each population expressed as a percent of the median observed with 40 nM α factor.

measures (**Supplementary Note** and **Supplementary Table 1** online). In general, the program identified all cells in a brightfield image with only a few spurious or 'false positive' cells (**Fig. 1a**, **Supplementary Note** and **Supplementary Fig. 1** online).

To identify cells, Cell-ID takes advantage of a distinct feature of brightfield images of yeast and other cell types. Notably, in images taken slightly below (100 nm) the focal plane, the boundary pixels were substantially darker than both the background of the visual field and the interior of the cell. The program identified cell boundaries as pixels whose grayscale values fell below a cutoff that the program determined automatically and independently for each image. The program then segmented the brightfield image into sets of contiguous pixels whose grayscale values were all above this cutoff. By using a brightfield image to find the cells instead of, for example, labeling the cells with a fluorescent protein and using a fluorescence image, we avoided bleaching the fluorophores, and we avoided scoring brighter or more uniformly fluorescent cells more efficiently. We also avoided a systematic error in the measurement of the cross-sectional area of the cells (and thus their volume, see **Supplementary Note**).

To illustrate the utility of finding cells in brightfield images, we altered Cell-ID to identify fluorescent protein–labeled cells from fluorescence images. For this fluorescent protein mode, we identified cells as sets of contiguous pixels above a threshold, three s.d. above the background of the fluorescence image. To compare both methods, we examined cells from a *MATa bar1Δ* strain in which a yellow fluorescent protein (YFP) open reading frame (ORF) replaced the chromosomal *PRM1* ORF, a gene induced by pheromone[17]. We induced expression of this gene with 20 nM pheromone for 30 min, halted protein translation by treatment with cycloheximide and allowed 3 h for fluorophore maturation. We found that the calculated cross-sectional area of untreated cells (where fluorescence is dominated by cellular autofluorescence) was similar for both methods (data not shown), but increased for cells identified using fluorescence images with respect to cells identified using brightfield images as cells accumulated fluorescent protein and became brighter (**Fig. 1b**).

Occasionally, for brightfield images, Cell-ID scored two nearby cells as a single cell. To address this problem, we developed an algorithm to identify pinch locations (bud necks or the location where two cells identified as one cell touched) and to quantify the degree to which the cells were pinched (**Supplementary Note** and **Supplementary Fig. 1**).

The segmentation algorithm should work well with cell types that are not highly irregular and produce dark outlines in brightfield images. We verified this with cells from the promyelocytic lymphoid human cell line HL-60 (refs. 18–20; **Fig. 1c**). Notably, Cell-ID was able to find these cells without modification to the code. However, the cell-splitting algorithm discussed above may need to be modified for HL-60 cells undergoing cytokinesis as the algorithm was tuned for budding yeast, where new cells appear as small and growing buds. Cell-ID can be altered to accommodate different methods and cell types. We compare the implemented Cell-ID algorithm with other segmentation methods in the **Supplementary Note**.

Measurement of total cell fluorescence

To quantify total cell fluorescence, we summed the signal from pixels associated with each cell, and then corrected for the non-cellular fluorescence background, photobleaching and light originating from out-of-focus regions of the cell (**Supplementary Note**). To determine how well this method measured small numbers of fluorescent protein derivatives, we replaced the chromosomal *STE5* ORF with different numbers of P_{STE5}-*YFP-STE5* genes (**Fig. 2**). In these strains YFP-Ste5 synthesis is under the control of the native *STE5* promoter (P_{STE5}). Ste5 (ref. 21) exists in approximately 500 molecules per cell (**Supplementary Note** and K.R. Benjamin *et al.*, unpublished data), and quantitative immunoblots (**Fig. 2a** and **Supplementary Note**) revealed that in the single-copy ("1×") strain, there are ~500 YFP-Ste5 fusion molecules as well.

We clearly distinguished fluorescence from cells with one copy of the P_{STE5}-*YFP-STE5* construct from cells that contained native *STE5* but no fluorescent derivative ("0×" strain; **Fig. 2b**). Because of the slow maturation of YFP (see below), the ~500 molecules of YFP-Ste5 in exponentially growing cells consisted of ~350 mature YFP fluorophores and ~150 not-yet-mature, and thus nonfluorescent, YFP molecules (**Supplementary Note**), indicating that we could quantify <350 fluorescent proteins. Our cells covered ~400

Table 1 | Sensitivity of the measurements

α factor (nM)	0	0.31	0.625	1.25	2.5	5	10	20	40
Microscopy	5	36.4	58.7	80.5	92.8	95.5	95.4	99.2	98.8
Flow cytometry	5	21.6	40.2	62.7	70.6	74.3	85.7	89.3	90.1

Indicated is the percentage of cells at the indicated dose of α factor that are bright enough to be distinguished from untreated (0 nM α factor) cells with 95% or better confidence. Maximum values (at the highest doses of α factor) are less than 100% because some cells exhibit low fluorescence even at high doses. These numbers depend on both the mean fluorescence of a population and on the dispersion around the mean. Microscope-based cytometry with Cell-ID exhibits better sensitivity, showing better separation from untreated cells at low doses of α factor.

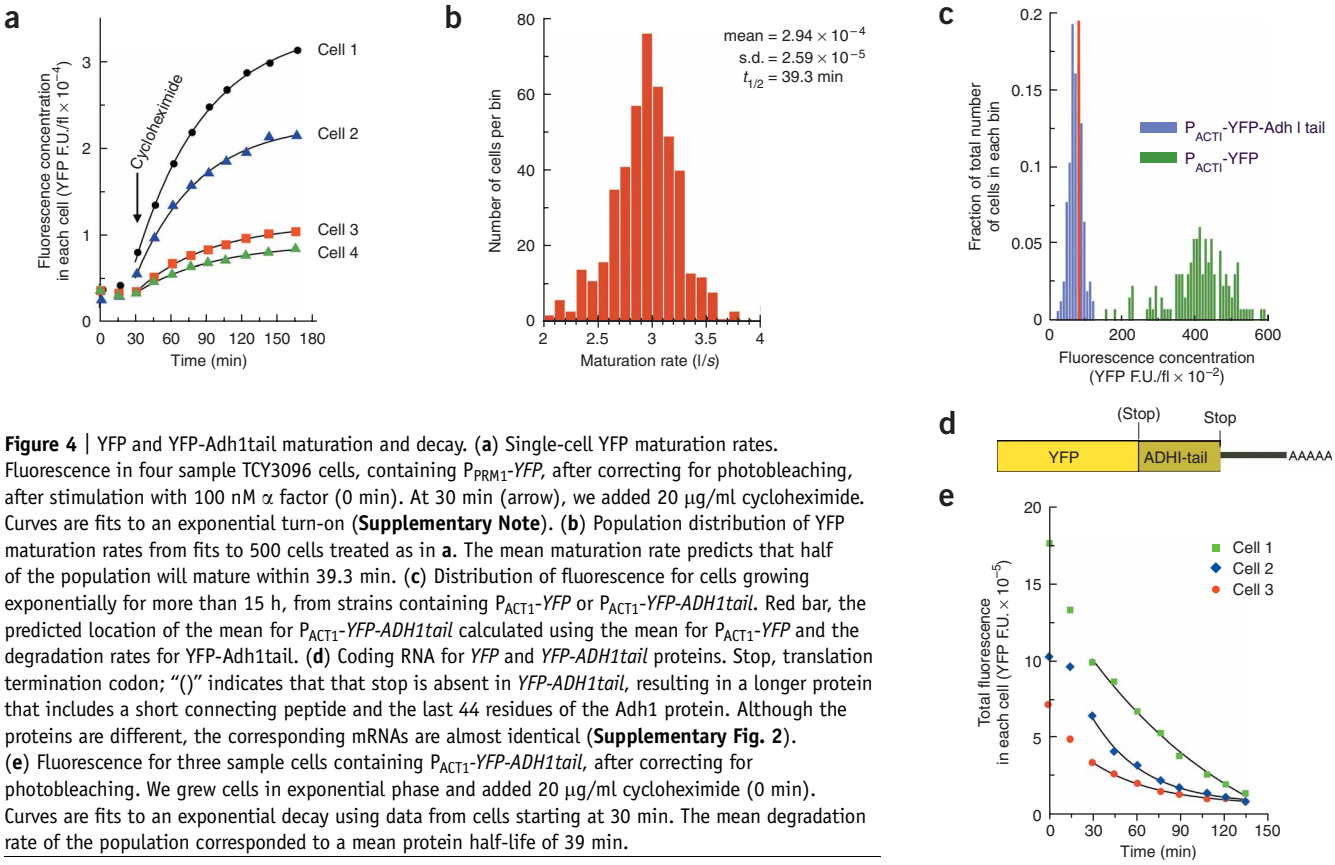

Figure 4 | YFP and YFP-Adh1tail maturation and decay. (**a**) Single-cell YFP maturation rates. Fluorescence in four sample TCY3096 cells, containing P_{PRM1}-*YFP*, after correcting for photobleaching, after stimulation with 100 nM α factor (0 min). At 30 min (arrow), we added 20 μg/ml cycloheximide. Curves are fits to an exponential turn-on (**Supplementary Note**). (**b**) Population distribution of YFP maturation rates from fits to 500 cells treated as in **a**. The mean maturation rate predicts that half of the population will mature within 39.3 min. (**c**) Distribution of fluorescence for cells growing exponentially for more than 15 h, from strains containing P_{ACT1}-*YFP* or P_{ACT1}-*YFP-ADH1tail*. Red bar, the predicted location of the mean for P_{ACT1}-*YFP-ADH1tail* calculated using the mean for P_{ACT1}-*YFP* and the degradation rates for YFP-Adh1tail. (**d**) Coding RNA for *YFP* and *YFP-ADH1tail* proteins. Stop, translation termination codon; "()" indicates that that stop is absent in *YFP-ADH1tail*, resulting in a longer protein that includes a short connecting peptide and the last 44 residues of the Adh1 protein. Although the proteins are different, the corresponding mRNAs are almost identical (**Supplementary Fig. 2**). (**e**) Fluorescence for three sample cells containing P_{ACT1}-*YFP-ADH1tail*, after correcting for photobleaching. We grew cells in exponential phase and added 20 μg/ml cycloheximide (0 min). Curves are fits to an exponential decay using data from cells starting at 30 min. The mean degradation rate of the population corresponded to a mean protein half-life of 39 min.

pixels in the CCD images, indicating that we could easily quantify roughly 1 fluorescent protein per pixel in living cells. As the distribution in the 1× strain is so distinct from that in the 0× strain, the true sensitivity limit is even lower. The dominant limitation on sensitivity is uncertainty in the autofluorescence of individual cells caused by cell-to-cell variation in autofluorescence. It is possible that illumination with wavelengths that excited autofluorescence but not YFP could be used for single-cell corrections. After correction for average autofluorescence, the two- and four-copy strains had two and four times the average fluorescence of the 1× strain (**Fig. 2c**). They also had, on average, two and four times the amount of YFP-Ste5 protein, as measured by immunoblotting (**Fig. 2a**). Thus, these fluorescence measurements increased linearly with the amount of the fluorescent protein derivative, even at small numbers of molecules per cell.

We compared these methods with analysis by one of the most sensitive presently available flow cytometers, a Becton-Dickinson LSR2. We examined induced fluorescence in cells that carried the pheromone inducible P_{PRM1}-*YFP* construct, which contains the YFP gene under the control of the *PRM1* promoter, at different pheromone doses. The population average of the microscope-acquired total fluorescence measurement agreed with the flow-cytometer measurements at all doses (**Fig. 3**). At low doses, where cells contained small numbers of fluorescent proteins, however, the microscope methods were able to separate populations of cells treated with one dose from populations treated with another better, and also were able to separate populations of untreated cells from treated cells better (**Table 1**).

Measurement of fluorophore maturation rate in single cells

We quantified maturation time[22,23] for YFP (wild-type GFP with mutations S65G,V68L,S72A,T203Y) and a cyan fluorescent protein derivative (CFP; wild-type GFP with mutations F64,S65T,Y66W,N146I,M153T,V163A), in individual *S. cerevisiae* at 25 °C (ref. 3; **Supplementary Note**). We induced fluorescent protein synthesis by addition of pheromone to cells with integrated constructs in which the fluorescent protein replaced the *PRM1* ORF, allowed transcription and translation to proceed for 30 min, then added cycloheximide to block translation. Cells reached maximum fluorescence by 3 h after translation stop (**Fig. 4a**); and photobleaching-corrected fluorescence (**Supplementary Note**) remained stable for up to 24 h (data not shown), indicating that under these conditions protein degradation was negligible.

Although individual cells varied in the total amount of YFP by a factor of four (**Fig. 4a**), there was little cell-to-cell variation in the maturation rates (**Fig. 4b**; coefficient of variation < 0.1; **Supplementary Note**). We performed an identical analysis for CFP (data not shown). In yeast under these conditions, YFP and CFP form mature fluorophores at similar rates, with average half-times for maturation of 39 ± 7 and 49 ± 9 min, respectively (**Supplementary Note**).

We use these measurements to understand our snapshot experiments immediately below. We have also used them elsewhere to

understand time courses of induction of fluorescent protein reporter genes[3].

Snapshot measurement of protein-degradation rates

In exponentially growing cells, the population average number of fluorescent protein derivatives (and other proteins) is constant over time[24,25]. Protein concentration depends on (i) production and degradation rates of the reporter mRNA, (ii) translation, maturation and degradation rates of the fluorescent reporter protein, and (iii) population doubling time[24–26] (**Supplementary Note**).

We compared exponentially growing cells in which the constitutive promoter P_{ACT1} drove expression of YFP to cells in which P_{ACT1} drove an unstable derivative, YFP-ADH1tail (**Supplementary Note**, **Fig. 4c**,**d** and **Supplementary Fig. 2** online). We calculated the ratio of the population average of total fluorescence per volume of YFP-ADH1tail to stable YFP to be 0.15 ± 0.02. Because both genes were integrated into the same site in the chromosome and had the same promoter, and because their mRNAs differed by only a few bases (**Fig. 4d** and **Supplementary Fig. 2**), we assumed that their mRNAs had the same rates of synthesis, translation and degradation, and thus that the ratio depended on doubling time, protein degradation rate and fluorophore maturation rate. We measured the increase in OD_{600} over time, determined the population doubling time to be 90 min for both strains and, from the experiments above, posited a degradation rate of 0 for YFP. We also made the assumption that the YFP domain of YFP-Adh1tail folded independently, so that the maturation rates for the YFP fluorophores in these two derivatives were identical. From these assumptions and the ratio 0.15 ± 0.02, we calculated a YFP-Adh1tail degradation rate of (3.45 ± 0.40) $\times 10^{-4}$ s^{-1} ($t_{1/2} = 33 \pm 4$ min; **Supplementary Note**).

We verified this result by performing experiments in which we measured the degradation rate after blocking translation with cycloheximide (**Supplementary Note** and **Fig. 4e**). We obtained a degradation rate of 3.0×10^{-4} s^{-1}, which is close to the value we calculated from the ratiometric snapshot experiments. This result suggests that we could generalize this single-image snapshot method to produce a high-throughput determination of degradation rates of a large collection of YFP fusion proteins in exponentially growing cells.

Snapshot measurement of an mRNA degradation rate

We then used the snapshot method to calculate the degradation rate of a native yeast mRNA. We compared the fluorescence from cells in which the *STE5* promoter drove a native, nonfused YFP (P_{STE5}-*YFP*) with strains in which the same promoter drove a YFP-STE5 fusion (P_{STE5}-*YFP-STE5*). Fluorescence from the YFP-Ste5 cells was roughly sixfold lower than from the YFP cells (**Fig. 2b**). Because both proteins were expressed from the same promoter, we assumed that this difference in fluorescence was not due to differences in transcription, but rather to differences in the stability of the mRNA or the protein.

Two experiments suggested that fluorescent protein–Ste5 derivatives were stable. In the first experiment we added cycloheximide to the P_{STE5}-*YFP-STE5* strain to stop protein translation and followed changes in fluorescence in single cells every 10 min for 3 h. Fluorescence per cell did not diminish (data not shown). In the second experiment, we used strains expressing GFP or GFP-Ste5 under the control of the inducible *GAL1* promoter. We induced expression by growing cells in 1% galactose and then switched expression off by addition of 2% glucose (**Supplementary Note**). After promoter shutoff fluorescence in both strains decreased in a manner quantitatively explained by protein dilution from cell proliferation, consistent with a lack of protein degradation (**Fig. 2d**).

The P_{STE5}-*YFP* and the P_{STE5}-*YFP-STE5* mRNAs had identical 5′ untranslated regions (**Supplementary Note**). We posited that these mRNAs were translated with equal efficiency and that the YFP mRNA was stable. Thus, the ratio of the average fluorescence concentration of P_{STE5}-*YFP-STE5* cells to P_{STE5}-*YFP* cells depended only on doubling time and mRNA degradation rates (**Supplementary Note**). We measured a fluorescence ratio of 0.17 and, from OD_{600} measurements, doubling times of 90 min (data not shown), which allowed us to calculate a *YFP-STE5* mRNA half-life of 18 min. This value agrees with a previously reported measurement of 14 min (12–17 min at 95% confidence) for *STE5* mRNA half-life[27].

DISCUSSION

In addition to the sensitive fluorescence measurements described here (sensitivity slightly better than one of the best-available flow cytometers), this combination of relatively simple microscope-based cytometric methods has also allowed us to measure loss of fluorescence resonance energy transfer (FRET) between regulatory proteins in the nucleus and relocalization of fluorescent proteins in response to pheromone system activation (R. Yu *et al.*, submitted) and to calculate correlations among several cellular variables (for example, cell volume, rate of volume increase and fluorescent-protein reporter output) to untangle and measure different sources of cell-to-cell variation after system activation[3].

Although we tuned Cell-ID to work with yeast cells, it readily identified mammalian lymphoid cells, which are regularly shaped and produce dark outlines in brightfield images. We believe the method Cell-ID used to separate incorrectly combined cells should work for other cell types with relatively regular features, such as bacteria or lymphocytes, but would require some modification for cells with more complicated processes, such as neurons and fibroblasts.

These methods allowed us to measure fluorescent protein fluorophore maturation rates *in vivo* in single cells. Although there was considerable cell-to-cell variation in the levels of fluorescent protein expressed, as expected[2,3], there was little (<10% of the mean) cell-to-cell variation in the maturation rates, consistent with the idea that maturation requires only intramolecular interactions[23,28] and may be mostly independent of the internal physiological state of the cells. We speculate that part of the small cell-to-cell variation may be caused by cell-to-cell differences in intracellular redox state.

Our "snapshot" calculations of protein and mRNA degradation rates required side-by-side comparison of single time point images of experiment and control cells in exponentially growing cultures. To justify the assumptions for these measurements, we measured protein stability by secondary experiments. In the future, however, we could build on the work of others[29] to obviate the need for secondary experiments. For example, for Ste5 we imagine a cell that expresses a CFP-ubiquitin(K48R)–YFP-Ste5 fusion. The CFP-ubiquitin(K48R) moiety should be rapidly cleaved from the YFP-Ste5

part of the protein by the cellular ubiquitin proteases to yield a stable protein, CFP-ubiquitin(K48R), which should serve as an internal control for YFP-Ste5 stability. Because both protein moieties are encoded by the same message, their relative fluorescence would be independent of the rate of mRNA degradation. By this means, we imagine that technically simple snapshot experiments could be scaled up to permit whole-genome measurements of mRNA and protein lifetimes, under different growth conditions, genetic modifications and experimental treatments. Because such measurements provide a means to measure steady-state mRNA and protein degradation rates in exponentially growing cells, they should complement pulse-chase[30–32], chemical synthesis inhibition[33], promoter shut off and temperature-shift synthesis inhibition experiments.

High-throughput optical microscope–based cytometry complements flow cytometry by allowing repeated measurements of the same cells over experimental time courses. Although there are commercial microscopy packages that provide considerable functionality, we believe that much important future methods development will involve open-source methods. Programs such as Cell-ID and CellProfiler provide means to extract information from fields of cells, and that data can be further analyzed by powerful packages such as PAW. The OME provides metadata standards for archiving and working with large numbers of images, and the μManager image acquisition software project will provide the ability to operate microscopes and associated devices. Combinations of such software should help future researchers quantify new features of biological image data.

METHODS

Construction of strains and plasmids. We detail construction of yeast strains and plasmids, and methods for quantifying proteins by western blots in the **Supplementary Note**.

Microscopy. To prepare yeast cells for microscopy, we maintained cultures in exponential growth for at least 15 h in BSM medium (Qbiogene, Inc.) with 2% glucose. To coat wells (96 MicroWell Optical Bottom Plate #1.5 Coverglass Base; Nalge Nunc International) with concanavalin A (type V; Sigma-Aldrich), we added to each well 100 μl of a 100 μg/ml solution of conA in water, incubated for 1 h at room temperature (18–23 °C), and then washed 3 times with water. We kept coated wells in water for up to 2 d before adding cells. After allowing 10 min for cells to settle and stick to the well bottoms, we washed away unbound cells. We maintained HL-60 cells at 37 °C and 5% CO_2 in RPMI 1640 medium (Invitrogen) supplemented with 10% FBS (Sigma-Aldrich) and 4 mM glutamine. Immediately before imaging, we transferred aliquots of cells to a 96-well glass-bottom plate.

To acquire images we used a 60× PlanApo objective with oil immersion (numerical aperture, NA = 1.4) in a Nikon TE2000 inverted microscope located in a 25 °C room. This microscope had automatic *z*-axis control, a motorized filter cube changer, a 100-W mercury arc lamp (HBO 100; Bulb Direct), brightfield and epifluorescence illumination electronic shutters (Uniblitz, Vincent Associates, and Smart Shutter, Sutter Instrument Company, respectively), a motorized *x-y* stage (MS-2000 stage, Applied Scientific Instrumentation), and a 512BFT MicroMax Peltier cooled CCD camera (Photometrix).

URL. μManager (http://www.micro-manager.org).

Note: Supplementary information is available on the Nature Methods website.

ACKNOWLEDGMENTS

We thank J. Newman for use of a Becton-Dickinson LSR2 flow cytometer, A. Arkin for supplying HL-60 cells, and P. Walter for use of a Zeiss LSM 510 confocal microscope. We also thank one of the reviewers for the idea of using Z-stack of confocal images to validate the volume measurements described in the **Supplementary Note**. Work was under the "Alpha Project" at the Center for Quantitative Genome function, a US National Institutes of Health Center of Excellence in Genomic Science. The Alpha Project is supported by grant P50 HG02370 to R.B. from the US National Human Genome Research Institute (NHGRI). The contents of this publication are solely the responsibility of the authors and do not necessarily represent the official views of the NHGRI.

AUTHOR CONTRIBUTIONS

A.G. wrote the relevant software and with A.C.-L., performed the data analysis and developed the microscopy methods. A.C.-L. carried out the wet-lab experiments. T.E.C. constructed the plasmids and yeast strains. K.R.B. quantified the YFP-Ste5 derivative by western blot. R.C.Y., A.C.-L. and A.G. calibrated the microscope-based fluorescence measurements. R.B. provided input into project design and interpretation of results. A.G., A.C.-L. and R.B. wrote the bulk of the paper.

COMPETING INTERESTS STATEMENT

The authors declare that they have no competing financial interests.

Published online at http://www.nature.com/naturemethods/
Reprints and permissions information is available online at http://npg.nature.com/reprintsandpermissions

1. Elowitz, M.B., Levine, A.J., Siggia, E.D. & Swain, P.S. Stochastic gene expression in a single cell. *Science* **297**, 1183–1186 (2002).
2. Raser, J.M. & O'Shea, E.K. Control of stochasticity in eukaryotic gene expression. *Science* **304**, 1811–1814 (2004).
3. Colman-Lerner, A. *et al.* Regulated cell-to-cell variation in a cell-fate decision system. *Nature* **437**, 699–706 (2005).
4. Rosenfeld, N., Young, J.W., Alon, U., Swain, P.S. & Elowitz, M.B. Gene regulation at the single-cell level. *Science* **307**, 1962–1965 (2005).
5. Pedraza, J.M. & van Oudenaarden, A. Noise propagation in gene networks. *Science* **307**, 1965–1969 (2005).
6. Shapiro, H.M. *Practical flow cytometry*. (Wiley-Liss, Hoboken, New Jersey, 2003).
7. George, T.C. *et al.* Distinguishing modes of cell death using the ImageStream multispectral imaging flow cytometer. *Cytometry A* **59**, 237–245 (2004).
8. Tarnok, A., Valet, G.K. & Emmrich, F. Systems biology and clinical cytomics: The 10th Leipziger Workshop and the 3rd International Workshop on Slide-Based Cytometry. *Cytometry A* **69**, 36–40 (2006).
9. Burns, N. *et al.* Large-scale analysis of gene expression, protein localization, and gene disruption in *Saccharomyces cerevisiae*. *Genes Dev.* **8**, 1087–1105 (1994).
10. Kahana, J.A., Schnapp, B.J. & Silver, P.A. Kinetics of spindle pole body separation in budding yeast. *Proc. Natl. Acad. Sci. USA* **92**, 9707–9711 (1995).
11. Sawin, K.E. & Nurse, P. Identification of fission yeast nuclear markers using random polypeptide fusions with green fluorescent protein. *Proc. Natl. Acad. Sci. USA* **93**, 15146–15151 (1996).
12. Elowitz, M.B. & Leibler, S. A synthetic oscillatory network of transcriptional regulators. *Nature* **403**, 335–338 (2000).
13. Huh, W.K. *et al.* Global analysis of protein localization in budding yeast. *Nature* **425**, 686–691 (2003).
14. Goldberg, I.G. *et al.* The Open Microscopy Environment (OME) Data Model and XML file: open tools for informatics and quantitative analysis in biological imaging. *Genome Biol.* **6**, R47 (2005).
15. Abramoff, M.D., Magelhaes, P.J. & Ram, S.J. Image processing with ImageJ. *Biophotonics International* **11**, 36–42 (2004).
16. Carpenter, A.E. *et al.* CellProfiler: image analysis software for identifying and quantifying cell phenotypes. *Genome Biol.* **7**, R100 (2006).
17. Heiman, M.G. & Walter, P. Prm1p, a pheromone-regulated multispanning membrane protein, facilitates plasma membrane fusion during yeast mating. *J. Cell Biol.* **151**, 719–730 (2000).
18. Collins, S.J. The HL-60 promyelocytic leukemia cell line: proliferation, differentiation, and cellular oncogene expression. *Blood* **70**, 1233–1244 (1987).
19. Xu, J. *et al.* Divergent signals and cytoskeletal assemblies regulate self-organizing polarity in neutrophils. *Cell* **114**, 201–214 (2003).
20. Darzynkiewicz, Z., Gorczyca, W., Lassota, P. & Traganos, F. Altered sensitivity of DNA *in situ* to denaturation in apoptotic cells. *Ann. NY Acad. Sci.* **677**, 334–340 (1993).

21. Dohlman, H.G. & Thorner, J.W. Regulation of G protein-initiated signal transduction in yeast. Paradigms and Principles. *Annu. Rev. Biochem.* **70**, 703–754 (2001).
22. Heim, R., Prasher, D.C. & Tsien, R.Y. Wavelength mutations and post-translational autoxidation of green fluorescent protein. *Proc. Natl. Acad. Sci. USA* **91**, 12501–12504 (1994).
23. Reid, B.G. & Flynn, G.C. Chromophore formation in green fluorescent protein. *Biochemistry* **36**, 6786–6791 (1997).
24. Subramanian, S. & Srienc, F. Quantitative analysis of transient gene expression in mammalian cells using the green fluorescent protein. *J. Biotechnol.* **49**, 137–151 (1996).
25. Leveau, J.H. & Lindow, S.E. Predictive and interpretive simulation of green fluorescent protein expression in reporter bacteria. *J. Bacteriol.* **183**, 6752–6762 (2001).
26. Monod, J., Pappenheimer, A.M., Jr. & Cohen-Bazire, G. The kinetics of the biosynthesis of beta-galactosidase in *Escherichia coli* as a function of growth. *Biochim. Biophys. Acta* **9**, 648–660 (1952).
27. Wang, Y. *et al.* Precision and functional specificity in mRNA decay. *Proc. Natl. Acad. Sci. USA* **99**, 5860–5865 (2002).
28. Tsien, R.Y. The green fluorescent protein. *Annu. Rev. Biochem.* **67**, 509–544 (1998).
29. Levy, F., Johnsson, N., Rumenapf, T. & Varshavsky, A. Using ubiquitin to follow the metabolic fate of a protein. *Proc. Natl. Acad. Sci. USA* **93**, 4907–4912 (1996).
30. Schoenheimer, R. & Rittenberg, D. The study of intermediary metabolism of animals with the aid of isotopes. *Physiol. Revs.* **20**, 218–248 (1940).
31. Rotman, B. & Spiegelman, S. On the origin of the carbon in the induced synthesis beta-galactosidase in *Escherichia coli*. *J. Bacteriol.* **68**, 419–429 (1954).
32. Hogness, D.S., Cohn, M. & Monod, J. Studies on the induced synthesis of beta-galactosidase in *Escherichia coli*: the kinetics and mechanism of sulfur incorporation. *Biochim. Biophys. Acta* **16**, 99–116 (1955).
33. Mandelstam, J. Turnover of protein in growing and non-growing populations of *Escherichia coli*. *Biochem. J.* **69**, 110–119 (1958).